Enhancing the FOCI extrapolation method by using a weighted least-squares approach

Al-Saleh, S. M., Margrave, G. F.

ABSTRACT

The *forward operator and conjugate inverse* (FOCI) method of wavefield extrapolation uses Wiener filtering to design nearly stable wavefield extrapolators, dual operator tables for evanescent filtering, and spatial downsampling of the lower frequencies to increase operator accuracy and decrease run times. In the current design of FOCI, the forward operator is simply a windowed version of the exact operator for a half step. The inverse operator is designed as a band-limited inverse of the first. The least-squares FOCI operator is formed as a convolution of the first operator with the conjugate of the second. As a final step, the least-squares operator may either be used directly or shortened with a Hanning window. The limitations of the first option are that the operator has to be long to ensure stability, and evanescent filtering can not be applied at every depth step where dual tables have to be used. On the other hand, while the second option gives short operators with evanescent filtering at every depth step where only one table is needed, short operators attenuate higher wavenumbers due to using a Hanning window. This limits its ability to handle deep steeply dipping events. In fact, most extrapolation methods can not design very short operators that can handle high angles of propagation and remain stable in a recursive scheme.

We introduce some enhancements to the current design by using a weighted least-squares approach. The weighted least-squares with transition band method changes the error criterion in a particular way to remove or reduce the overshoot at discontinuities separating the propagating and evanescent regions. This approach is used to obtain the forward operator instead of using a Hanning window, and to obtain the windowed operator, instead of the Hanning window, in an optimal way. With these enhancements to FOCI, it is possible to design operators as short as 9 points. The migration results obtained with these enhancements show that short operators can generate good images very efficiently.

INTRODUCTION

Wavefield extrapolation methods extend the exact constant-velocity phase-shift extrapolators in the wavenumber-frequency domain to approximate space-frequency domain extrapolators suitable for laterally varying velocities. The major reason to express the algorithm in the space frequency domain is to obtain computational speed, and this requires developing a compactly supported (i.e. finite length) approximation to the theoretical response, which is infinitely long. The design of a space-frequency operator from the theoretical wavenumber-frequency expression is often done using a Taylor series expansion, but least-squares optimizations have also been used. For example, Holberg (1988) uses non-linear least squares, Hale (1991) uses novel basis functions in the wavenumber domain, Soubaras (1996) uses the Remez exchange algorithm to achieve equiripple behavior in the wavenumber domain, Thorbecke et al. (2004) use weighted least-squares with a modified transition region, Margrave et al.

(2005) introduced the *forward operator and conjugate inverse* (FOCI) method that splits the operator into two parts using one to stabilize the other, and Al-Saleh et al. (2005) used a transition band for the transition region in the weighted least square design of wavefield extrapolators instead of a specific transition function as in Thorbecke et al. (2004).

The Fourier transform of the ideal extrapolator has a discontinuous derivative at the boundary separating the propagating and evanescent regions. Thus, changing the ideal transform to remove these slope discontinuities makes the approximation easier and more accurate. Further, using a weight function puts more weight on the wavenumber band of interest to make the approximation a better match to the ideal in that region (Al-Saleh et al., 2005; Parks and Burrus, 1987). By using a transition band in the weighted least-squares design, the new error criterion removes or reduces the overshoot at the evanescent boundary. This is achieved by removing a region from the optimization, which is called a transition band.

In this report, we use weighted least-squares with a transition band (WLSTB) to enhance the FOCI algorithm. We begin with a short theoretical review of the FOCI algorithm followed by the theory of these enhancements. Then follows a series of examples and comparisons between the old and new designs beginning with operator amplitude and phase spectra, moving on to impulse responses, and finally to pre-stack depth migration. The full migrations are all done with the 2-D acoustic Marmousi model.

THEORY

Wavefield extrapolation in 2D can be done as a spatial convolution in the $\omega - x$ (temporal frequency and lateral spatial coordinate) domain using (Margrave and Ferguson, 1999; Margrave et al., 2005; Al-Saleh et al., 2005)

$$\psi\left(x, z+\Delta z, \omega\right) = \int_{-\infty}^{\infty} \psi\left(x', z, \omega\right) W\left(x-x', k\left(x\right), \Delta z\right) dx', \tag{1}$$

where the $\omega - x$ wavefield extrapolator W is given by

$$W\left(x-x', k\left(x\right), \Delta z\right) = \frac{1}{2\pi} \int_{-\infty}^{\infty} \hat{W}\left(k_x, k\left(x\right), \Delta z\right) e^{-ik_x\left(x-x'\right)} dk_x . \tag{2}$$

ψ is the pressure wavefield after taking its Fourier transformation over the temporal coordinate, $\hat{W}$ represents the symbol of W, $k\left(x\right) = \omega / v\left(x\right)$, z is depth, Δz is the depth increment, x is the transverse coordinate, ω is the temporal frequency, k_x is the transverse wavenumber, x' denotes the transverse coordinate at input, and x denotes the transverse coordinate at output.

The convolution in equation 1 becomes non-stationary when the velocity varies with x, and stationary when the velocity is constant. In our notation, velocity enters implicitly through $k = \omega / v$, and this is denoted as the second dependent variable for W. The non-stationary convolution operator, $W\left(x-x', k\left(x\right), \Delta z\right)$, handles lateral velocity variations

by using a different operator for each output point. In equation 2, $W\left(x-x',k(x),\Delta z\right)$ is infinitely long; that is, it is not compactly supported. The FOCI algorithm can be used to find a nearly stable approximation to $W\left(x-x',k(x),\Delta z\right)$ that has a compact support by which equation 1 can be approximated.

Stability here means that after m repeated applications of applying $\tilde{W}$ (the approximated operator) in a recursive scheme in a homogeneous medium, $\left|\hat{\tilde{W}}\right|^m \le \left|1+\varepsilon\right|^m \sim 1+m\varepsilon$, where '^' means the Fourier transform over the spatial coordinate. When $\varepsilon = 0$, then $\tilde{W}$ is perfectly stable and technically non-stable otherwise. However, if $m\varepsilon \ll 1$, then $\tilde{W}$ is practically stable. The region $k(x) \ge k_x$ is called the propagating region while the region $k(x) < k_x$ is called the evanescent region. In the propagating region, the Fourier transform of the ideal extrapolator yields $\left|\hat{W}\right| = 1$, but gives $\left|\hat{W}\right| < 1$ in the evanescent region.

The FOCI algorithm uses two useful properties of $\hat{W}$

$$\hat{W}\left(k_x,k(x),\Delta z\right) = \hat{W}\left(k_x,k(x),\frac{\Delta z}{2}\right)\hat{W}\left(k_x,k(x),\frac{\Delta z}{2}\right) \tag{3}$$

and

$$\hat{W}^{-1}\left(k_x,k(x),\frac{\Delta z}{2}\right) = \hat{W}^{*}\left(k_x,k(x),\frac{\Delta z}{2}\right),\ k_x < k(x) \tag{4}$$

where "*" indicates the complex conjugate. Next, let $\tilde{W}(\Delta z/2)$ be a compactly supported approximation (where the functional dependence has been suppressed except for Δz) as in

$$\tilde{W}(\Delta z/2) = \Omega\left(n_{for}\right)W(\Delta z/2), \tag{5}$$

where Ω is a Hanning window of length n_{for}. The FOCI algorithm then seeks another compactly supported operator $\tilde{W}_I$ such that

$$\tilde{W}_I \bullet \tilde{W}(\Delta z/2) = F^{-1}\left[\left|\hat{W}(\Delta z/2)\right|^{\eta}\right], \tag{6}$$

where F^{-1} symbolizes the inverse Fourier transform over k_x, the bullet denotes spatial convolution, and $0 \le \eta < 2$ is an adjustable parameter. The function of the right hand side of equation 6 is a zero-phase bandlimited approximation to a delta function. If $\eta = 0$, then the right hand side is truly a delta function and hence $\tilde{W}_I$ will be an exact inverse of

$\tilde{W}(\Delta z/2)$. On other hand, when $\eta > 0$, $\tilde{W}_I$ will be a band-limited inverse of $\tilde{W}(\Delta z/2)$. Since $\tilde{W}(\Delta z/2)$ has the half that phase of $\tilde{W}(\Delta z)$, and since $\tilde{W}_I$ has the opposite phase of $\tilde{W}(\Delta z/2)$, the FOCI approximation to $W(\Delta z)$ is

$$W_F(\Delta z) = \tilde{W}_I^* \bullet \tilde{W}(\Delta z/2) \approx W(\Delta z) \tag{7}$$

which follows from the approximate inverse nature of $\tilde{W}_I$ and from equations 3 and 4. Equation 7 shows that the FOCI operator can be assembled from the convolution of an approximate forward operator with the conjugate of its bandlimited inverse: hence the acronym FOCI. Since both $\tilde{W}(\Delta z/2)$ and $\tilde{W}_I$ are compactly supported by design then so is $W_F(\Delta z)$.

In the current design of the FOCI extrapolator, the phase accuracy is limited by the initial estimate of the forward operator for a half step, $\tilde{W}(\Delta z/2)$. The bandlimited inverse obtained by solving equation (6) can, at best, negate this phase. The parameter η (equation 6) controls the degree of evanescent filtering in the final composite operator $W_F(\Delta z)$ (equation 7). For $\eta = 0$, the resulting $W_F(\Delta z)$ is all-pass (no evanescent filtering), while for $\eta = 2$, $W_F(\Delta z)$ has strong evanescent filtering. Since evanescent filtering is not needed at every depth step, dual operator tables are used in depth migration, the first table with strong evanescent filtering and a second with very little (Margrave et al., 2005). This corresponds to the choice of two different η values (equation 6) when constructing these tables. Then, for most extrapolation steps, the second table corresponding to a small η is used, but for every j_{th} step, the first table with large η is used. Moreover, the length of $W_F(\Delta z)$ in samples is given by $n_{op} = n_{for} + n_{inv} - 1$ where n_{for} = *length of* $\tilde{W}(\Delta z/2)$ and n_{inv} = *length of* $\tilde{W}_I(\Delta z/2)$. Further, a post-design shorter operator can be obtained by multiplying the final operator with a Hanning window as in

$$W_H(\Delta z) = \Omega(n_{win}) W_F(\Delta z), \tag{8}$$

where n_{win} is the length of the post-design operator. Note that in the current design of FOCI, $\tilde{W}(\Delta z/2)$ and $W_H(\Delta z)$ are obtained in a suboptimal way. To make optimal approximations and hence increase the stability of this method, we introduce the following enhancements:

i) Weighted least-squares approach to approximate $\tilde{W}(\Delta z/2)$.

ii) Weighted least-squares approach to obtain $W_H(\Delta z)$.

Using a weighted least square approach for the forward operator

Instead of using a Hanning window to truncate the forward operator (equation 5), which is suboptimal, we use weighted least-squares. The 1D discrete Fourier transform over the spatial coordinate of the forward operator is given by

$$\hat{\tilde{W}}\left(m\Delta k_x, \omega, \Delta z/2\right) = \Delta x \sum_{n=-(N-1)/2}^{(N-1)/2} \tilde{W}\left(n\Delta x, \omega, \Delta z/2\right) e^{im\Delta k_x n\Delta x} \tag{9}$$

and

$$\Delta k_x = \frac{2\pi}{M\Delta x}, \tag{10}$$

where M is the number of samples of the Fourier transform, and N is the number of filter coefficients (Thorbecke et. al., 2004). The ideal extrapolation operator $\hat{W}$ is symmetric with respect to k_x, which implies that the complex-valued extrapolation filter coefficients of $\tilde{W}$ should be even. This also means that

$$\tilde{W}\left(x_n\right) = \tilde{W}\left(x_{-n}\right), \tag{11}$$

This even-symmetry requirement suggests that N should be odd with the coefficient index, n, bounded by (Hale, 1991)

$$-(N-1)/2 \le n \le (N-1)/2\,. \tag{12}$$

To obtain a least-squares solution, $M > N$, so that there are more equations than unknowns. Equation 9 can also be expressed in matrix notation as

$$\underline{\hat{\tilde{W}}} = \underline{F}\,\underline{\tilde{W}}\,, \tag{13}$$

where F is the appropriate M by N subset of the Fourier transformation matrix. A weighted least-squares solution is given by (Parks and Burrus, 1987; Thorbecke, 2004)

$$\underline{\tilde{W}}_{LS} = \left[\underline{F}^H \Upsilon \underline{F}\right]^{-1} \underline{F}^H \Upsilon \underline{\hat{W}}\,, \tag{14}$$

where the superscript H denotes the complex-conjugate transpose, $\Upsilon\left(k_x\right)$ is a non-negative error weighting function, and the subscript LS indicates the least-squares approximation. In this method of weighted least-squares, a transition band is used for the transition region so that the desired transform does not have discontinuities (Parks and Burrus, 1987; Selesnick et. al., 1996). In other words, the band of wavenumbers for the transition region is simply removed from the error definition, and the region is called the transition band or "don't care" band. Moreover, the weight function puts much more weight on the propagating region than the evanescent region. The error function becomes

$$E = \sum_{m=-(M-1)/2}^{(M-1)/2} \Upsilon\left(k_x\right)\left|\hat{W}\left(m\Delta k_x, \omega, \Delta z/2\right) - \hat{\tilde{W}}\left(m\Delta k_x, \omega, \Delta z/2\right)\right|^2, \tag{15}$$

where

$$\Upsilon\left(k_x\right) = \begin{cases} 1 & \left|k_x\right| \le k_\alpha \\ 0 & k_\alpha < \left|k_x\right| < \left|2k - k_\alpha\right| \\ \varepsilon & \left|2k - k_\alpha\right| < \left|k_x\right| < \dfrac{\pi}{\Delta x} \end{cases}, \tag{16}$$

such that

$$\varepsilon \ll 1, \tag{17}$$

where $k_\alpha = \left(k \sin\alpha\right)$ and α is the maximum propagation angle , $k = f / v$, and ε is the weight for the evanescent regions. There is no constraint placed on $\hat{W}\left(k_x, \omega, \Delta z / 2\right)$ in the transition region. The forward extrapolator can be obtained using

$$\underline{\tilde{W}}_{LS} = \left[\underline{F}^H \Upsilon \underline{F}\right]^{-1} \underline{F}^H \Upsilon \underline{\hat{W}}. \tag{18}$$

We then modify equation (6) to read

$$\tilde{W}_{ILS} \bullet \tilde{W}_{LS}\left(\Delta z / 2\right) = F^{-1}\left[\left|\hat{W}\left(\Delta z / 2\right)\right|^{\eta}\right]. \tag{19}$$

Once this is solved by standard (unweighted) least–squares for $\tilde{W}_{ILS}$, the revised FOCI least-squares operator can be calculated using

$$W_{FLS}\left(\Delta z\right) = \tilde{W}^*_{ILS} \bullet \tilde{W}_{LS}\left(\Delta z / 2\right) \approx W\left(\Delta z\right) \tag{20}$$

Using a weighted least-squares approach for the post-design operator

The same optimization can be carried in the same way to obtain the windowed operator,

$$W_{HLS} = \left[\underline{F}^H \Upsilon \underline{F}\right]^{-1} \underline{F}^H \Upsilon \underline{\hat{W}}_{FLS}, \tag{21}$$

where $\underline{\hat{W}}_{FLS}$ is the spatial Fourier transform of W_{FLS} obtained from equation 20. This approach enables us to calculate very short operators that remain practically stable in a recursive scheme.

ANALYSIS

We will show the effect of these enhancements at three stages of the FOCI design

i) The improvement on the approximate forward operator.

ii) The improvement on the FOCI least-squares operator.

iii) The improvement on the post-design operator.

Figure 1.a shows the difference between the current design of calculating the forward operator, $\tilde{W}$, and the effect of using weighted least-squares with transition band (WLSTB) where the desired response is shown for comparison. The amplitude of $\hat{\tilde{W}}_{LS}$ shows more stability than the amplitude of $\hat{\tilde{W}}$. This shows that using WLSTB can be more effective to in obtaining a better design for the forward operator. The phase spectra are shown in Figure 1.b where the phase of $\hat{\tilde{W}}_{LS}$ shows a better approximation to the phase of the desired transform than the phase of $\hat{\tilde{W}}$. Figure 2.a shows a comparison of the amplitudes of the desired transform, $\hat{W}_F$ (old FOCI design), and $\hat{W}_{FLS}$ (with WLSTB) and the phases are shown in Figure 2.b. The amplitude of $\hat{W}_{FLS}$, the enhanced operator, shows greater stability than the old design which used weighted least-squares for the forward operator. The oscillatory behavior of the phase of $\hat{W}_{FLS}$ in Figure 2.b in the evanescent region is a direct result of using weighted least-squares where most of the weight is put on the wavelike region, and it can oscillate in the band that has lesser importance.

Next, we will show some comparisons of FOCI and FOCI with WLSTB on poststack and prestack examples. Our post-stack algorithm is a standard exploding reflector depth migration. Our pre-stack algorithm uses the shot-record migration paradigm and the deconvolution imaging condition

$$r(x,z) = \frac{\psi_{data}(x,z)\psi^{*}_{shot}(x,z)}{\psi_{shot}(x,z)\psi^{*}_{shot}(x,z) + \xi}, \qquad (22)$$

Where $\psi_{data}(x,z)$ is the downward extrapolated data to a depth z, $\psi^{*}_{shot}(x,z)$ is the forward modeled source, '*' is the complex conjugated, and ξ is a small positive stability constant.

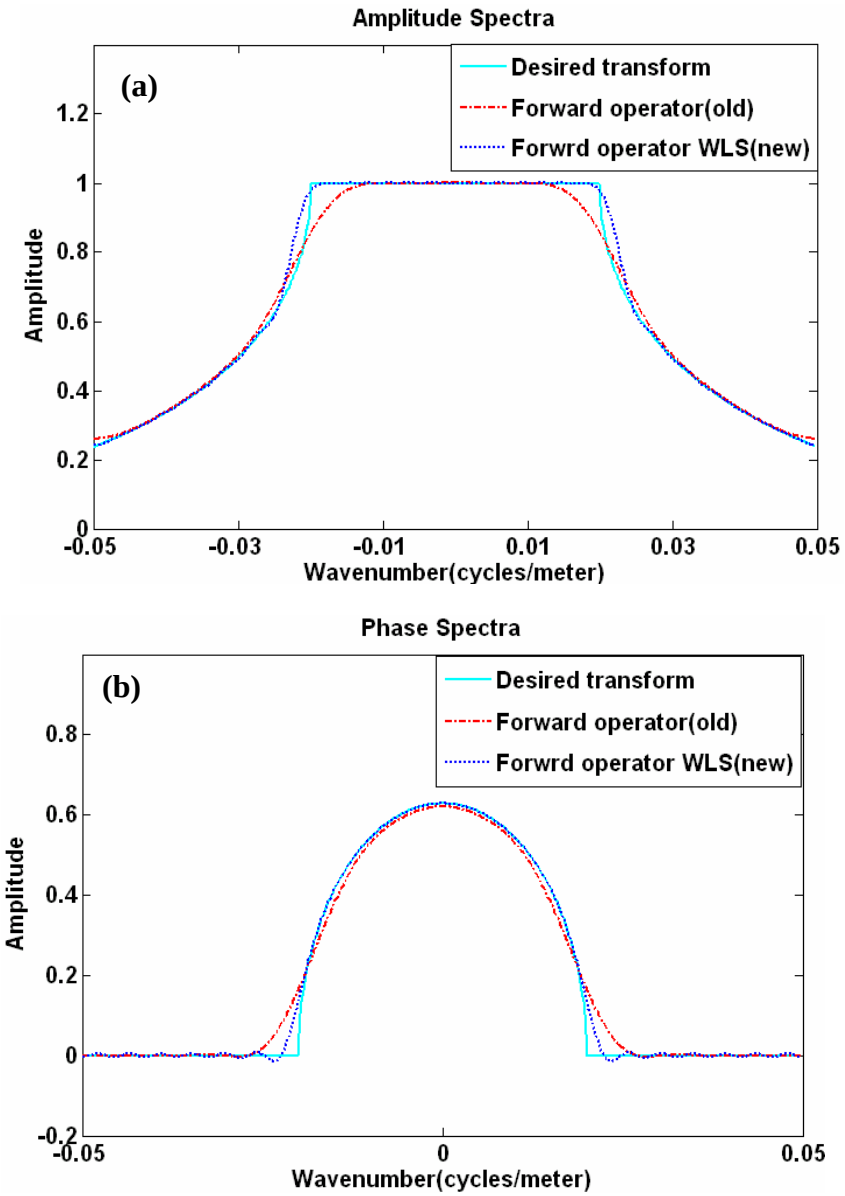

FIG. 1. (a) Amplitude spectra of the desired transform of the exact operator, Fourier transform of the forward operator that is obtained by a truncation with a Hanning window, Fourier transform of the forward operator obtained with weighted least square with a transition band (WLSTB). (b) Phase spectra of the Fourier transform of the exact operator, the forward operator obtained with a Hanning window, and the forward operator obtained with WLSTB. The parameters employed are $\Delta x = \Delta z = 10\text{m}$, $f = 40$ Hz, and $n_{fow} = 21$.

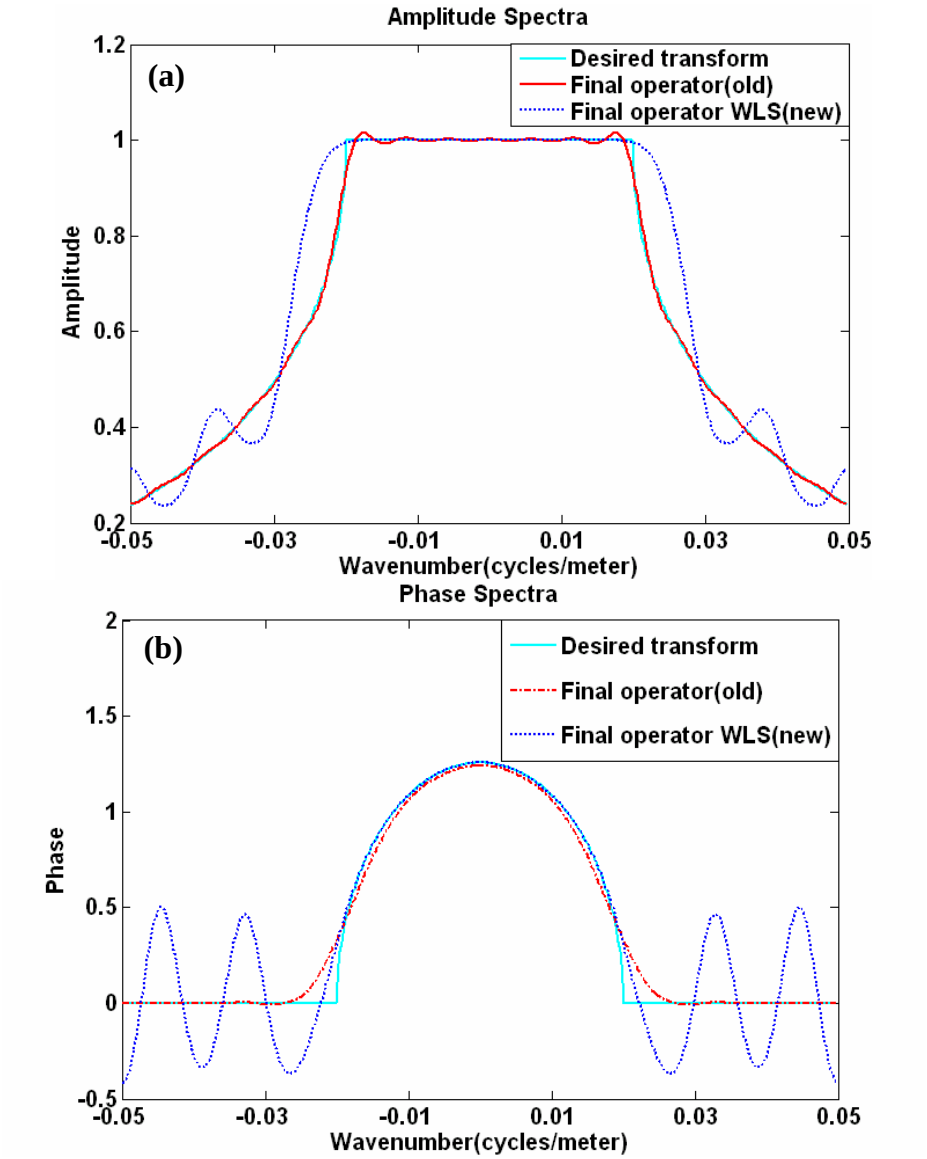

FIG. 2. (a) Amplitude spectra of the desired transform of the exact operator, Fourier transform of the final operator that is obtained by FOCI, Fourier transform of the final operator obtained with weighted least square with a transition band (WLSTB). (b) Phase spectra of the Fourier transform of the exact operator, the final operator, and the final operator obtained with WLSTB. The parameters employed are $\Delta x = \Delta z = 10\text{m}$, $f = 40\,\text{Hz}$, $n_{fow} = 21$, $n_{ninv} = 31$, $\eta = 1$, and $n_{op} = 51$.

However, in the original design of FOCI, the calculated operator with η=1 is only used for evanescent filtering applied every 10 or 20 depth steps. The operator that is mostly used for extrapolation is obtained with small η such as 0.01. As a result, dual operator tables are needed for extrapolation and evanescent filtering (Margrave et al., 2005). Moreover, spatial resampling that is used by FOCI helps to increase the stability of the operators where during the wavefield extrapolation process, the data is divided into frequency chunks that are optimally resampled in the spatial coordinates to enhance the performance of the extrapolation. As frequency decreases or velocity increases, the operators might have poor phase control as the operator wavenumbers will fall in the evanescent region. The full theory of spatial resampling is beyond the scope of this report and can be found in Margrave et al. (2005). However, we will show its importance using Figure 3. The amplitudes of the operators are shown in Figure 3.a compared with the desired transform. After spatial resampling, the operator is more stable than before. Also, the phases of the operators before and after spatial resampling are shown in Figure 3.b where the phase control better matches the phase of the desired transform. This example shows that operators corresponding to low frequencies or high velocities will have improved performance after spatial resampling. All these factors such as the dual tables and spatial resampling explain the good images that were obtained by FOCI with long operators.

The other enhancement to FOCI is by using a WLSTB approach to obtain the post-design operator. The current design uses a Hanning window to obtain a post-design short operator as in equation 8.

Despite the good images of this operator on Marmousi data (Al-Saleh et al., 2005; Margrave et al., 2005); it required a long operator such as 51 points. When we use the same design to obtain a shorter operator such as 15 points, it decays for some wavenumbers (Figure 4.a) and it does not have an accurate phase (Figure 4.b). However, with the WLSTB enhancement, we can obtain short operators that remain stable in a recursive scheme. This operator can be designed using

$$\underline{W}_{HLS} = \left[\underline{F}^H \Upsilon \underline{F} \right]^{-1} \underline{F}^H \Upsilon \hat{\underline{W}}_{FLS}, \qquad (23)$$

Figure 4.a shows a comparison between the amplitudes of $\hat{W}_H$ and $\hat{W}_{HLS}$ compared with the desired transform. The amplitude of $\hat{W}_{HLS}$ shows that it can migrate steeper dips than the old design. Further, it has much better phase control (Figure 4.b).

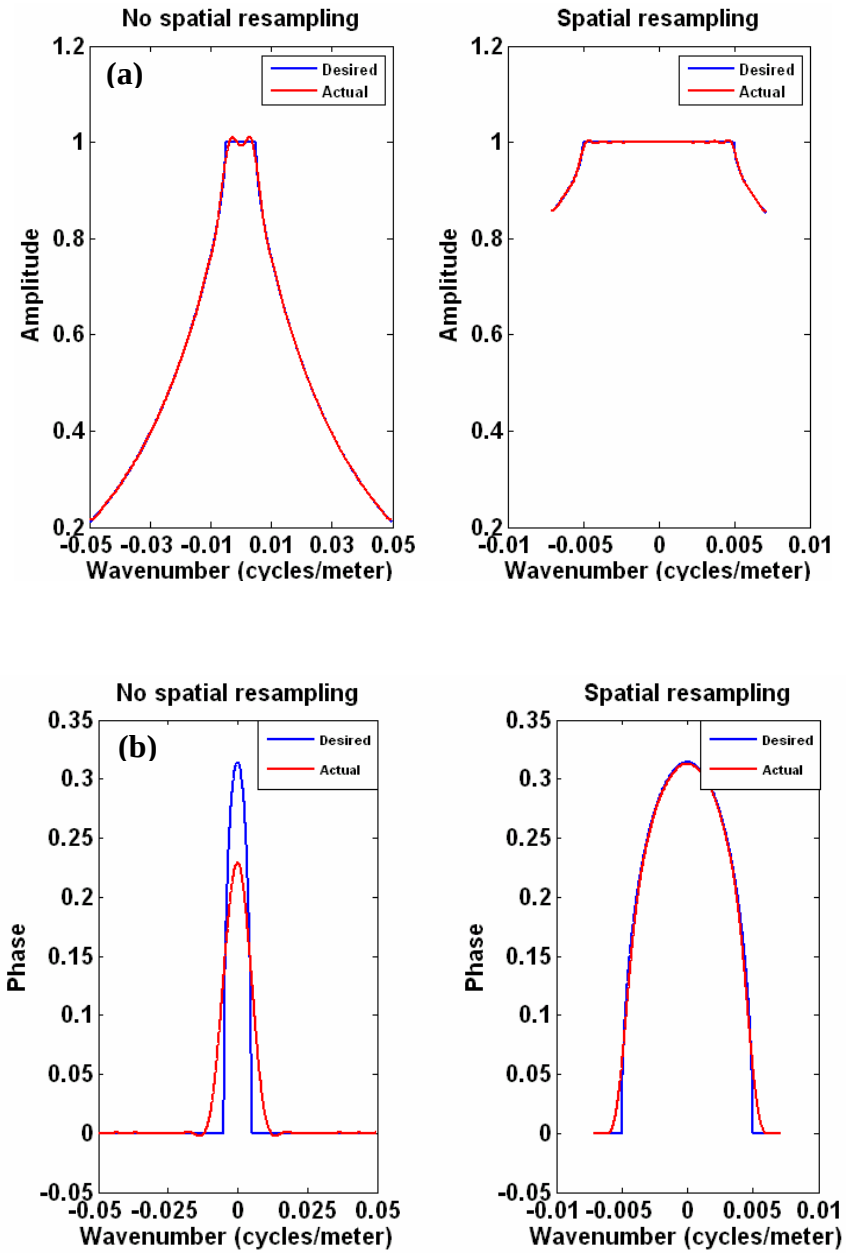

FIG. 3. The effect of spatial resampling on the stability and accuracy of (a) the amplitude and (b) the phase of the operator compared with the desired transforms. The parameters employed are $\Delta x = \Delta z = 10\text{m},\ \Delta x' = 70\text{m},\ f = 10\text{Hz},\ n_{fow} = 21,\ n_{ninv} = 31,\ \eta$=1, and $n_{op} = 51$where $\Delta x'$ is the new spacing after resampling.

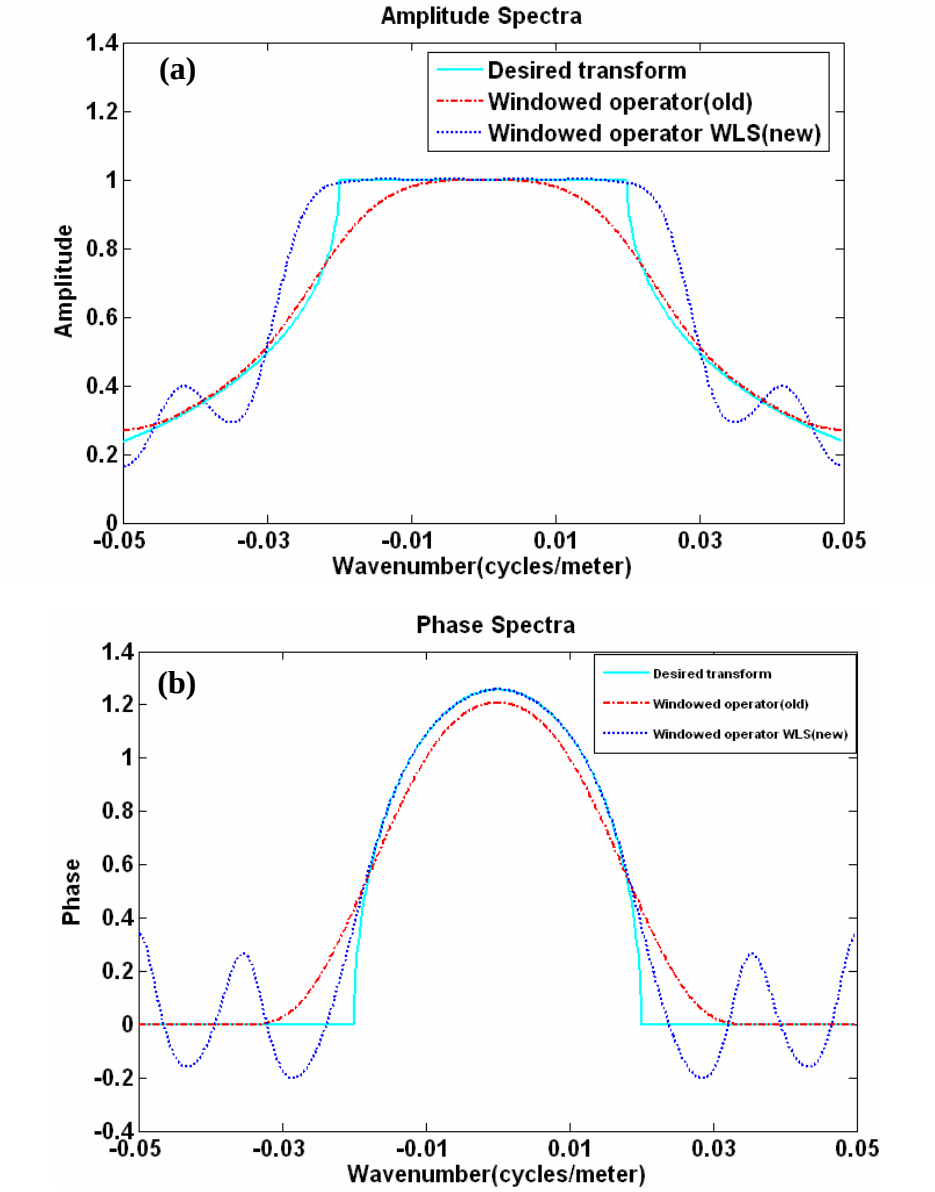

FIG. 4. Post-design operators without and with WLSTB, where (a) shows the amplitude spectra and (b) shows the phase spectra. The parameters are $\Delta x = \Delta z = 10\text{m}$, $f = 40\text{Hz}$, $n_{fow} = 21$, $n_{ninv} = 31$, $\eta = 1$, and $n_{win} = 15$.

IMPULSE RESPONSE EXAMPLES

Figure 5 shows a comparison of the impulse responses of post-stack implementations of the phase-shift algorithm, the FOCI algorithm, and FOCI with the WLSTB enhancement. The input was a set of six impulses on the center trace, the velocity was 4000 m/s, and the trace spacing and the depth step were both 10 m. The enhancement of FOCI with the weighted least-squares approach has improved the response over the old design of FOCI. The operator length of these results is 15 points obtained using equation 23. The enhanced FOCI operator was more effective in handling the higher angles of propagation (Figure 5.b) than the operator that was obtained with a Hanning window (Figure 5.a).

PRESTACK DEPTH MIGRATION OF MARMOUSI DATASET

We have conducted a series of tests of the enhanced FOCI algorithm with the enhancement in imaging the Marmousi structure with pre-stack depth migration. The results are compared with the old design of FOCI. The 2-D acoustic Marmousi dataset was created at the Instut Francais du Petrole (IFP) (Bourgeois et al., 1991). With the presence of complex reflectors, steep dips and strong velocity gradients, it is widely recognized as an ideal synthetic dataset for testing migration algorithms. The dataset consists of 240 individual shot records of 96 traces each in a marine, towed streamer, configuration. The source and receiver intervals are 25 m and the highest coherent frequencies in the data are about 50 Hz. Prior to migration, we applied a wavelet shaping filter designed to whiten the signal spectrum and to remove an approximately 60 ms delay due to ghosting and water-bottom multiples. We also interpolated each shot to a receiver spacing of 8.3333 m. Figure 6.a shows an approximation to the Marmousi reflectivity. The reflectivity was calculated using $r(x,z) = -\mathrm{sgn}\left(\frac{\partial}{\partial z}\ln v(x,z)\right)\left|\tilde{\nabla}\ln v(x,z)\right|$. The migration results of FOCI and FOCI with WLSTB are shown in Figures 6.b and 6.c. It is apparent that the image in Figure 6.c is in better agreement with the reflectivity in Figure 6.a. Figure 7.a shows a close-up of the central part of Figure 6.a and Figures 7.b and 7.c shows close-ups of Figures 6.b and 6.c. These demonstrate that we can see much more detail with FOCI using WLSTB with this short operator. The operator length is 15 points obtained from $n_{inv} = 31,\ n_{for} = 21,\ n_{win} = 15$ for both results. This enhancement enables us to obtain even further short operators. Figure 8 shows the migration result with $n_{inv} = 31,\ n_{for} = 21,\ n_{win} = 9$. Even with this short operator, a good image for Marmousi can be obtained. This enhancement shows that the FOCI algorithm can now generate good images with very short operators.

Figure 9 shows different comparisons of FOCI versus FOCI with WLSTB with different operator lengths. For example, Figure 9.a shows close-ups of the best image obtained using FOCI with $n_{win} = 51$, and Figure 9.b shows the same parts but obtained with the enhanced algorithm using the same operator length. They are similar but more detail is visible with the enhancement. As the operator length decreases to 15 points (Figure 9.c), we can still see good detail even with a 9-point operator (Figure 9.d). Figure

10 shows the runtimes of six migration results with six operator lengths. This figure shows that shorter operators are computationally more efficient than long operators.

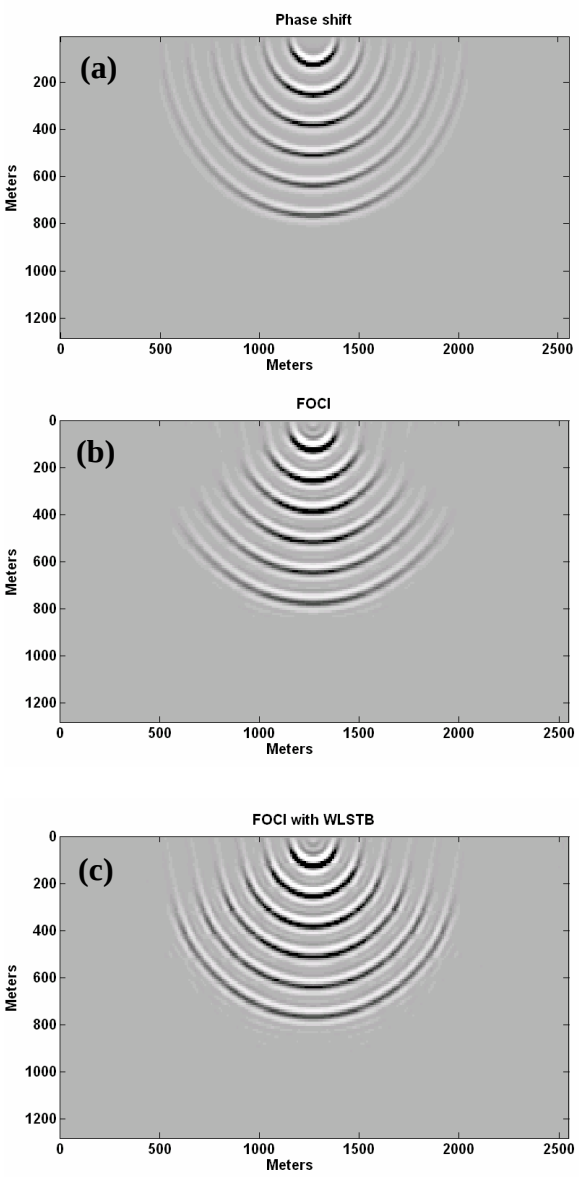

FIG. 5. Impulse responses of (a) phase shift migration, (b) FOCI, and (c) FOCI with WLSTB. The parameters are $\Delta x = \Delta z = 10$ m, $\Delta t = 0.004$ ms, $n_{for} = 101$, $n_{ninv} = 121$, $\eta = 1$, and $n_{win} = 15$.

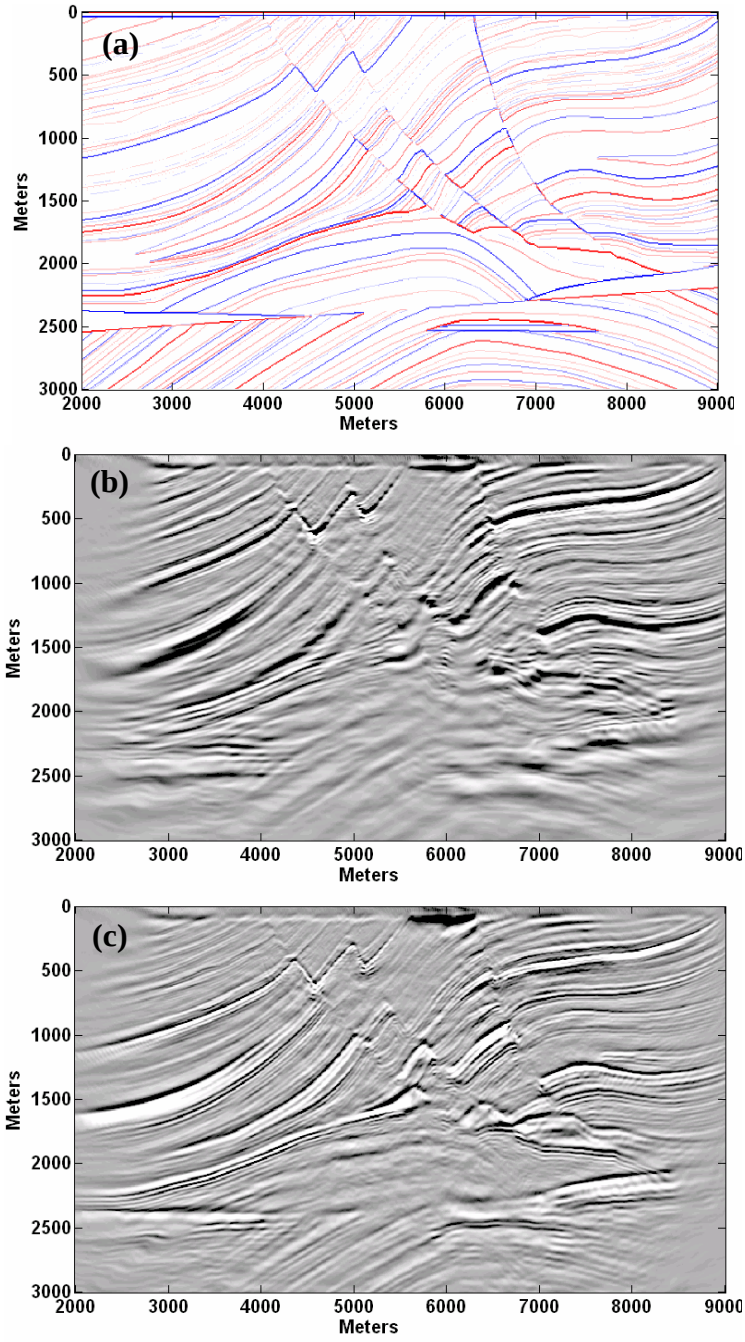

FIG. 6. Prestack depth migration results of Marmousi dataset where (a) shows the reflectivity, (b) shows the result with the current design of FOCI, and (c) shows the result of FOCI with the weighted least-squares enhancement. The parameters are $\Delta x = \Delta z = 8.3333$ m, $\Delta t = 0.004$ ms, $n_{fow} = 21$, $n_{ninv} = 31$, $\eta = 1$, and $n_{win} = 15$.

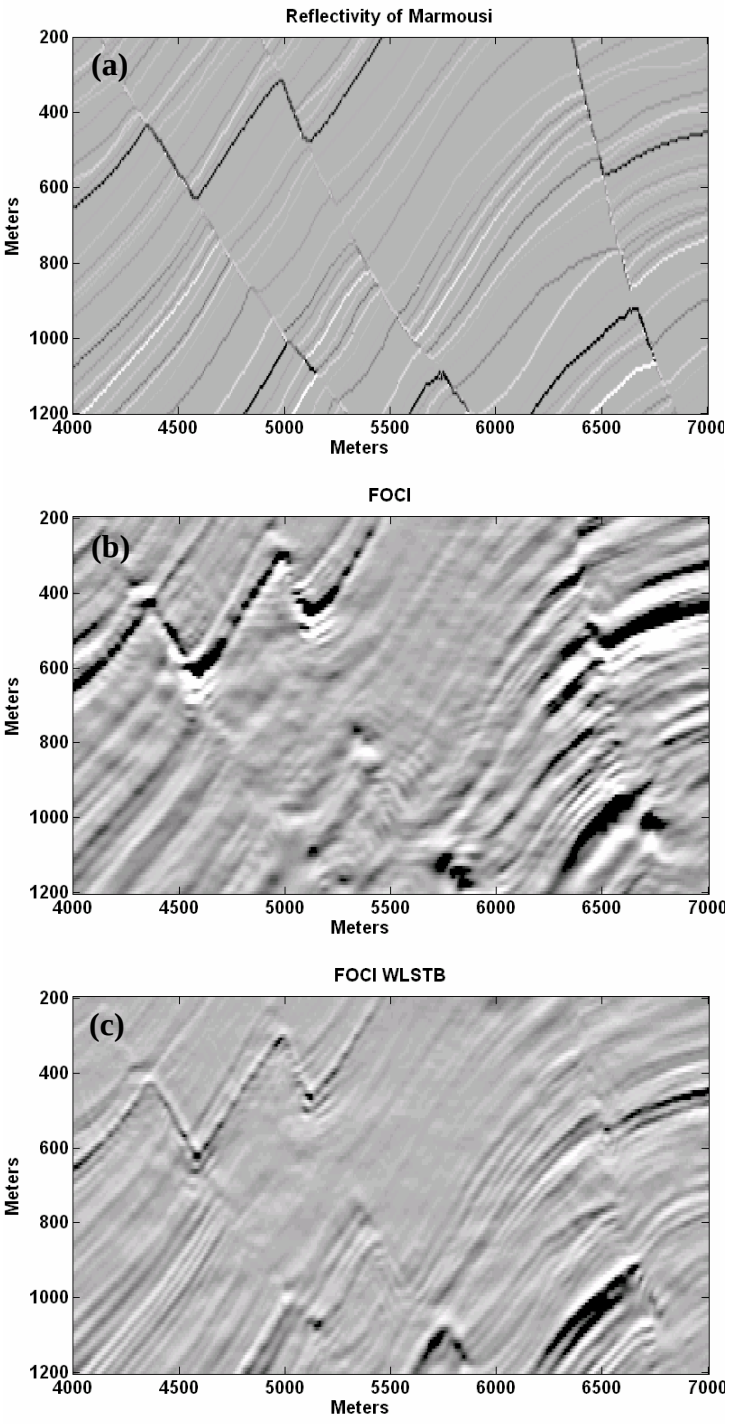

FIG. 7. Close-up views of the shallow central sections of Figures 6.a, 6.b, and 6.c.

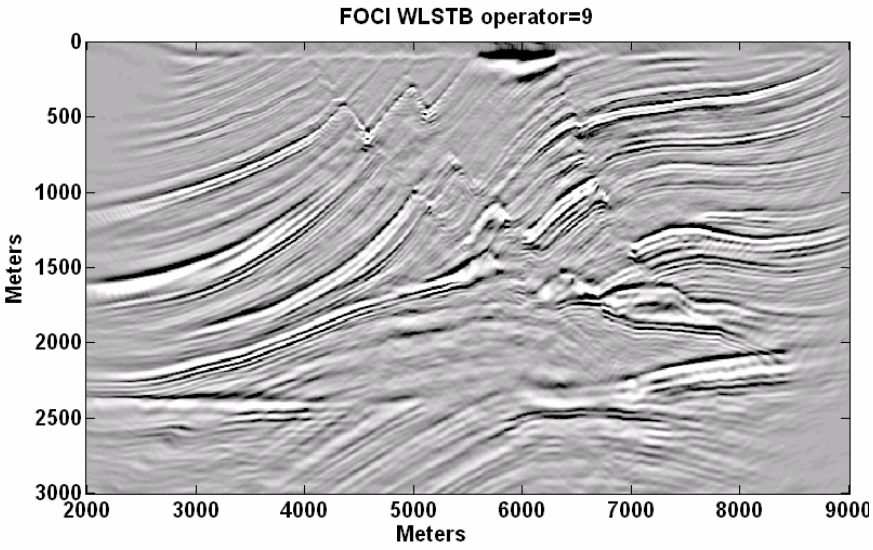

FIG. 8. Prestack migration result obtained with the enhanced FOCI algorithm with a 9 point operator.

CONCLUSIONS

The *forward operator and conjugate inverse* (FOCI) algorithm uses Wiener filtering and spatial resampling to design wavefield extrapolators that remain practically stable in a recursive scheme. The FOCI algorithm required long operators to generate good images. Enhancing the FOCI algorithm with weighted least-squares using a transition band for the transition region; enables one to design short operators that remained practically stable in a recursive scheme. In this approach of weighted least-squares, the region that connects the wavelike and evanescent regions is simply removed from the optimization by applying a zero-weight to it. This region, the transition band, contains the discontinuities, which are a potential source for instability.

Enhancing FOCI with weighed least-squares eliminates the need for dual tables for evanescent filtering since the operator can attenuate the evanescent energy very effectively. With this enhancement, FOCI is now even more computationally efficient due to its ability to be designed with short operators.

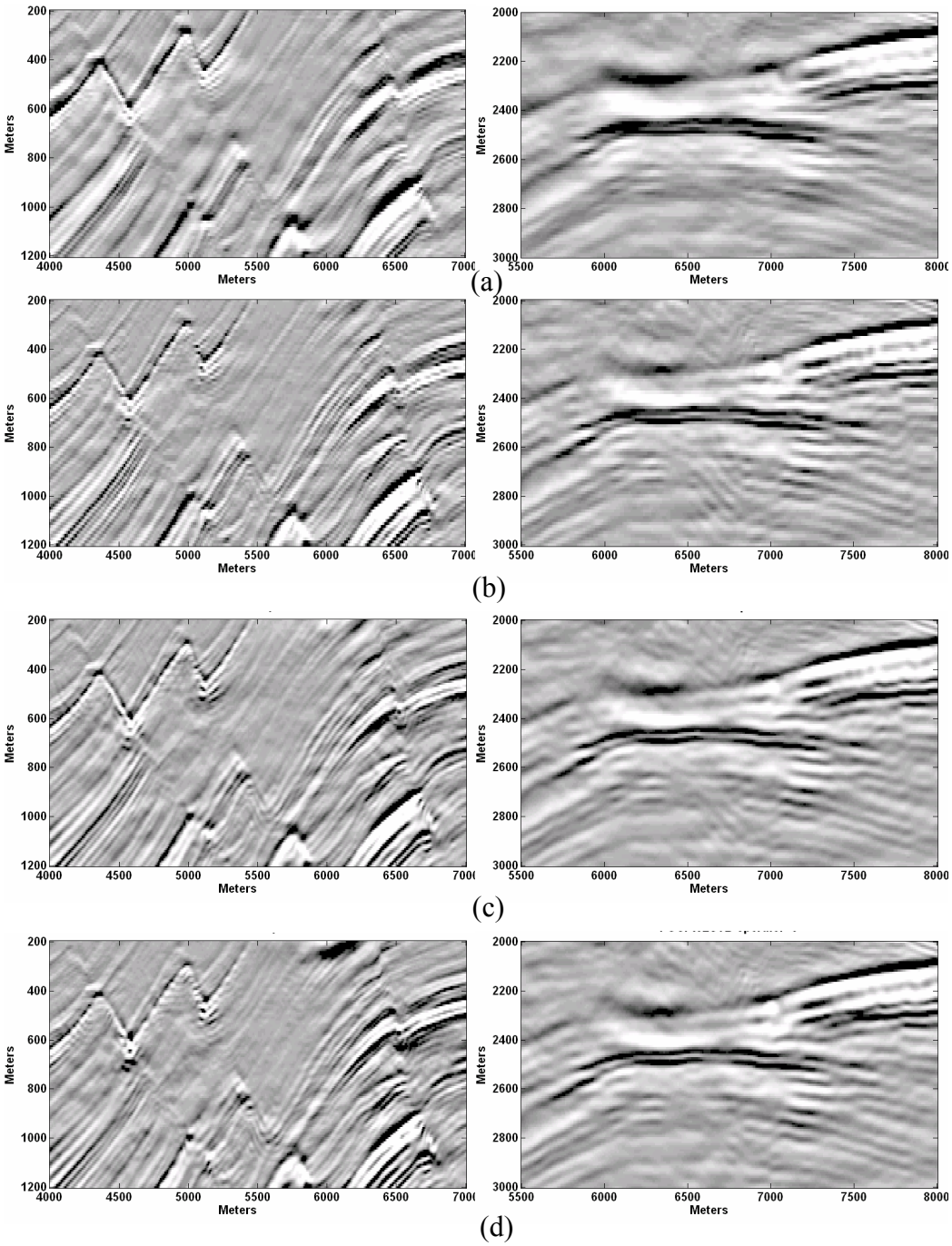

FIG. 9. Comparisons of FOCI before and after the enhancement at zoomed sections with various operator lengths where (a) is obtained from FOCI (old design) with $n_{win} = 51$, (b) is obtained from FOCI with WLSTB using $n_{win} = 51$, (c) is obtained from FOCI with WLSTB using $n_{win} = 25$, and (d) is obtained from FOCI with WLSTB using $n_{win} = 9$.

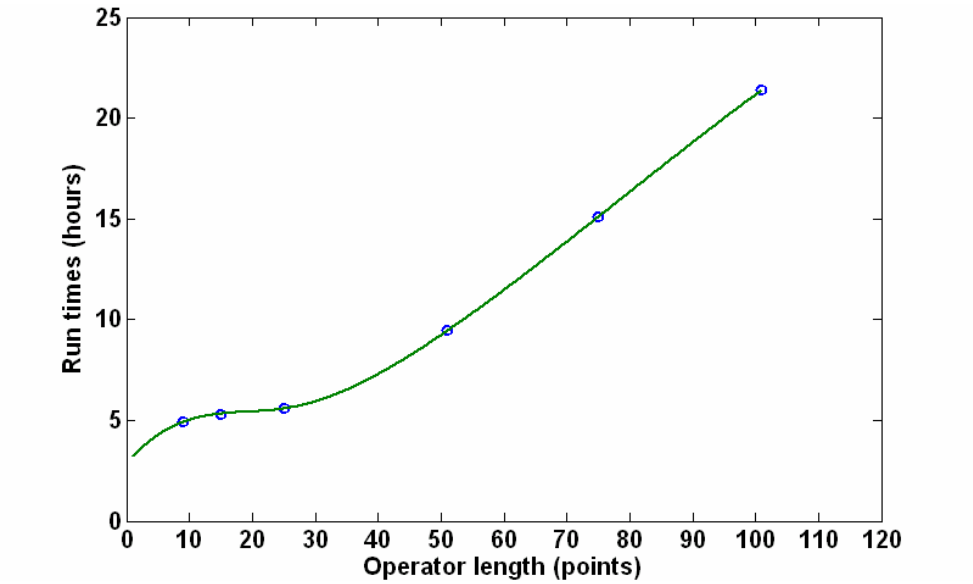

FIG. 10. Runtimes versus operator lengths where $\Delta x = \Delta z = 12.5$ m, and $\Delta t = 0.004$ ms.

REFERENCES

Al-Saleh, S. M., and Margrave, G. F., and Bancroft J.C., 2005, Using a transition band in the weighted least square design of wavefield extrapolators, This volume.

Bourgeois, A., Bourget, M., Lailly, P., Poulet, M., Ricarte, P. and Versteeg, R., 1991, Marmousi, model and data: in Versteeg, R. and Grau, G. (editors), 1991, The Marmousi experience, Proceedings of the 1990 EAGE workshop on practical aspects of seismic data inversion, EAGE, p5-16.

Hale, D., 1991, Stable explicit depth extrapolation of seismic wavefield, Geophysics, **56**, 1770-1777.

Holberg, O., 1988, Towards optimum one-way wave propagation, Geophys. Prosp., **36**, 99-114.

Margrave, G. F. and Ferguson, R. J., 1999, Wavefield extrapolation by nonstationary phase shift: Geophysics, **64**, 1067-1078.

Margrave, G.F., Geiger, H.D., Al-Saleh, S., and Lamoureux, M.P., 2005, Improving explicit depth migration with a stabilizing Wiener filter and spatial resampling: submitted to Geophysics

Parks, T.W., and C.S. Burrus, 1987, Digital Filter Design, John Wiley & Sons, pp. 54-83.

Selesnick, I.W., Lang, M., and Burrus, C.S., 1996, Constrained Least Squares Design of FIR Filters with Specified Transition Bands, IEEE, **44**, 1879-1892.

Soubaras, R., 1996, Explicit 3-D migration using equiripple polynomial expansion and Laplacian synthesis, Geophysics, **61,** 1386-1393.

Thorbecke, J., Wapenaar, K., and Swinnen, G., 2004, Design of one-way wavefield extrapolation operators, using smooth functions in WLSQ optimization, Geophysics, **69**, 1037-1045.

ACKNOWLEDGEMENTS

We wish to thank the sponsors of the CREWES project and the POTSI project. We also specifically thank NSERC, MITACS, and PIMS for providing funding and other support. We would like also to thank Saudi Aramco Oil Company. We also thank Chuck Ursenbach for his comments and suggestions.